IEEE Access
Multidisciplinary | Rapid Review | Open Access Journal

Received 13 March 2024, accepted 28 March 2024, date of publication 3 April 2024, date of current version 11 April 2024.

Digital Object Identifier 10.1109/ACCESS.2024.3384606

RESEARCH ARTICLE

Broadband Waveguide-to-Differential-Line Transition in Multi-Layer Substrates With Triple Stacked Patch in 300 GHz Band

CHATCHAI CHOKCHAI, (Graduate Student Member, IEEE), YOSHIKI SUGIMOTO, (Member, IEEE), KUNIO SAKAKIBARA, (Senior Member, IEEE), HENRY ABU DIAWUO, AND NOBUYOSHI KIKUMA, (Senior Member, IEEE)

Department of Electrical and Mechanical Engineering, Nagoya Institute of Technology, Nagoya 466-8555, Japan

Corresponding author: Yoshiki Sugimoto (sugimoto.yoshiki@nitech.ac.jp)

This work was supported by the Ministry of Internal Affairs and Communications of Japan through a Scheme of Research and Development for Expansion of Radio Wave Resources under Grant JPJ000254.

ABSTRACT A broadband waveguide-to-differential-line transition with a triple stacked patch is proposed for use in 300 GHz band. This transition consists of differential signal lines inserted into the waveguide region from both broad walls of the waveguide. A triple circular stacked patch element was used for broadband transmission from the waveguide to the planar differential line formed in a multi-layer substrate. Concurrently, the optimized arrangement of via holes can prevent electric field leakage efficiently and improve the transmission characteristic in a high-frequency band. The geometry of the transition was optimized through electromagnetic simulations using the finite element method. Measurements and simulations were implemented to evaluate the performance of the transition. The measured result of the transition shows the bandwidth of the S_{11} below -10 dB was over 100 GHz.

INDEX TERMS Differential line, multi-layer substrate, stacked patch, terahertz band, transmission line, transition, waveguide.

I. INTRODUCTION

Terahertz (THz) technologies have received considerable attention owing to their high-frequency bands with extensive bandwidths. The data transmission rate and speed increase in gigabits [1], [2], [3]. The development of signal-encryption techniques for transmitting data and modulating amplitude-shift keying (ASK) signals has been presented [4]. The photo-mixer has accompanied the results of modulation techniques to achieve a greater bandwidth [5]. The KIOSK data-download system was developed as an application for high-speed wireless communication systems [6]. Wireless communication systems have been continually evolved, and terahertz technologies have been introduced for the sixth-generation mobile communication systems [7], [8]. Owing to their superiority in the high angular resolution of terahertz frequencies, it has been enhanced for automotive sensor systems operating in the 300 GHz band [9]. The connection between radio frequency (RF) circuits and antennas significantly affects the signal-to-noise (S/N) ratio. Therefore, waveguide interfaces without interference between the antennas and RF circuits have been developed [10], [11].

To reduce the significant loss of wireless systems in this frequency range, design techniques for antennas integrated with RF circuits and embedded in packages with devices have been applied. Monolithic microwave integrated circuit (MMIC)-to-antenna connection techniques have also been proposed [12]. Microstrip lines, coplanar waveguides (CPW), and grounded coplanar waveguides (GCPW) are the transmission lines that are commonly used on the top metal planes of multi-layer substrates to connect with an IC. Depending

The associate editor coordinating the review of this manuscript and approving it for publication was Li Yang.

on the circuit configuration of the applications, differential and single-ended lines can be used for IC connections. The transitions of transmission lines are critical for connecting planar transmission lines to waveguides to maximize power transmission and minimize loss. Waveguide transitions from both differential and single-ended lines must be designed to prevent loss owing to the balun, depending on the application. Differential lines are essential in connecting differential circuits and rectangular waveguides, owing to differential line advantages in anti-interference. Therefore, both single-ended and differential-line-to-waveguide transitions have evolved.

Over the past few years, single-ended-line-to-waveguide transitions have been continuously progressed. The back-short transition with a wide operating bandwidth is one of the most popular transitions [13], [14], [15]. The metal top cap must be accurately assembled on the substrate, which causes fabrication problems. Therefore, transitions without back-short structures were developed using a GCPW feed to mitigate the structural problems of back-short transitions. However, its bandwidth is essentially narrow [16], [17]. Microstrip-to-waveguide transitions with a rectangular patch, which is a simple structure, were proposed [18], [19], [20], [21]. The design methodology for a waveguide to two microstrip lines transition using a rectangular patch was proposed in reference [22]. Recently, the types of transitions that have gained recognition are the E-shaped patch element [23], slot coupling technique in multi-layer substrates [24], V-shaped patch element [25], via-less with choke structure transitions [26], [27], rectangular patch with the positioning of the via-hole to control the transmission mode [28], and via fence and air hole matching structures [29], [30]. CPW to air-filled rectangular waveguide transition using a rectangular radiator etched with a semi-elliptic slot [31]. Suspended stripline to air-filled rectangular waveguide transition with a U-shaped patch [32]. On the other hand, the air-filled transition has the disadvantage of difficulty in fabrication. Substrate integrated suspended line (SISL) to rectangular waveguide with a T-shaped patch [33]. The most popular approach for increasing bandwidth is the stacked double-patch configuration [34], [35].

Both single-ended and differential lines are typically used at IC terminals. Differential-line-to-waveguide transitions connect a differential line to a waveguide to avoid the loss of area-consuming baluns. The differential-line-to-waveguide transitions support a direct connection between the differential microstrip line and rectangular waveguide [36] A waveguide-to-stripline transition uses a dual-frequency response technique to increase bandwidth [37]. The hollow waveguide-to-differential-line transition on a multi-layer dielectric substrate in the 300 GHz band using patch and window dimensioning techniques for increasing the bandwidth was offered [38]. In [39], a differential microstrip line (DML)-to-rectangular waveguide transition with wide bandwidth was proposed. A differential-line-to-waveguide transition with a short-ended slot line using the differential line as the ground-signal-signal-ground technique (GSSG) and waveguide blocks has been presented [40]. A waveguide-to-differential-line transition has also been proposed [41]. The waveguide-to-differential-line transition in a multi-layer substrate was presented in [42] and [43]. In the core and prepreg layers, when electromagnetic waves pass through multiple substrates, multiple resonances can occur, thereby increasing the bandwidth.

The excitation technique for the waveguides is essential for the efficiency and bandwidth of the transition. Many techniques, such as aperture excitation, have been applied to waveguides [44]. Broadband techniques have been developed using waveguide taper [45], back-short structure [46], fin-line taper [47], unilateral substrateless finline structure [48], and differential line inserted from the narrow wall of the waveguide with X-shaped patch [49]. In addition, the development of this transition depends on its implementation in applications.

As mentioned above, most waveguide-to-differential-line transitions are designed for low frequencies and narrow bandwidths. In addition, the feed direction is limited due to the polarization in the rectangular waveguide. Therefore, there remains a challenge for existing designs to achieve broadband in terahertz band. A comparison with our previous work [49], the transition using a differential line inserted from the narrow wall of the waveguide and multi-resonance of the X-shaped patch used for broadband operation. However, the bandwidth was insufficient to fully cover the WR-3 band. With the difference in design and principle, this work can achieve higher performance with a frequency bandwidth of 100 GHz, covering the full WR-3 band. This paper proposes a broadband waveguide-to-differential-line transition covering the WR-3 band based on the principle of multimode resonance in a cavity. Broadband operation is accomplished through a combination of techniques, a triple circular stacked patch, and the utilization of multiple resonances within the circular cavity formed by a via-hole arrangement with apertures patterned in a multi-layer substrate. The differential lines are located on the top layer of the multi-layer substrate, where IC chips can be mounted. The differential lines are inserted from the broad wall of the waveguide. The TE_{10} mode on L8 of the rectangular waveguide transforms into the TE_{11} mode within the quasi-circular waveguide on L6 and L7. Subsequently, the TE_{11} mode from Patch 1 transforms into the quasi-TEM mode on the differential lines. Then, multimode resonance in a cavity produces broadband operation.

The remainder of this paper is organized as follows. The design and structure of the circular cavity, triple circular patch, and via-hole arrangement are described in Section II. The verification of the transition simulations by numerical validation via electromagnetic analysis using the finite element method (Ansys HFSS) is presented in Section III. Experimental results on the feasibility of the proposed design technique are presented in Section IV. Finally, the conclusions of the study are presented in Section V.

II. CONFIGURATION OF PROPOSED TRANSITION

This section describes the configuration and the design of the proposed waveguide-to-differential-line transition. Microstrip-to-waveguide transitions can offer broadband performance across a broad frequency spectrum while maintaining low insertion losses. The purpose of developing this transition is to establish a connection between the 265 GHz CMOS circuit receiver and the WR-3.4 waveguide interface in a multi-layer substrate [10], [11]. Multi-layer substrates provide the flexibility to integrate various passive and active components. Utilizing the specified core materials, these substrates offer the advantage of enabling the transition's use in intricate circuits requiring multiple routing layers. The multi-layer substrate consists of eight copper plates separated by seven dielectric plates, with three prepreg layers on each side of the core layer. It is produced using a high-pressure heating process. The modified semi-additive process (MSAP) achieves micropatterns with fine pitches [50]. These micropatterns are gold-plated with a thickness of 0.05 μm, following a 4 μm nickel layer application on the copper plate interface. MSAP imparts rounded corners to the metal patterns, with a 10 μm corner radius. The accuracy of metal patterns on the same layer is 10 μm, whereas on different layers, it is 25 μm. Additionally, the signal line pattern width maintains an accuracy of $\pm$10 μm.

A. CONFIGURATION AND PRINCIPLE

The rectangular structure will produce errors with rounded corners, so a comparatively circular structure reduces the frequency shifts due to rounded corner errors and a more compact size at the same frequencies. The circular cavity structure was chosen for This paper because a circular cavity possesses a high degree of geometric symmetry, and the circular cross-section of the cavity inherently encourages the formation of multiple resonance modes.

The transition consists of three parts: a triple-stacked patch arrangement in the circular cavity structure and a via hole arrangement to block the electric field leakage in the high band. The cavity structure in a multi-layer substrate consists of a main TE_{10} and TE_{11} dual-mode cavity. The concept behind this cavity structure is founded on utilizing three cavity resonance modes. The cavity structure is configured in an hourglass shape. The circular aperture sizes transition from small to large from L5–L7, whereas they shift from large to small from L2–L5. Specifically, L5 features the smallest apertures. On the other hand, L8 is distinguished by rectangular apertures, primarily due to its connection to the waveguide. Grounded coplanar waveguides (GCPW) are used as differential signal lines. The differential signal lines are inserted into the waveguide region on top of L1 from both broad walls of the waveguide, as shown in Fig. 1. The TE_{10} mode propagates in the bottom waveguide and inputs into the substrate from the aperture on the metal L8. The electromagnetic wave passes through all apertures on all metal layers. Three patches on L2, L4, and L5 were placed at the middle of the apertures to control the electromagnetic coupling between the apertures.

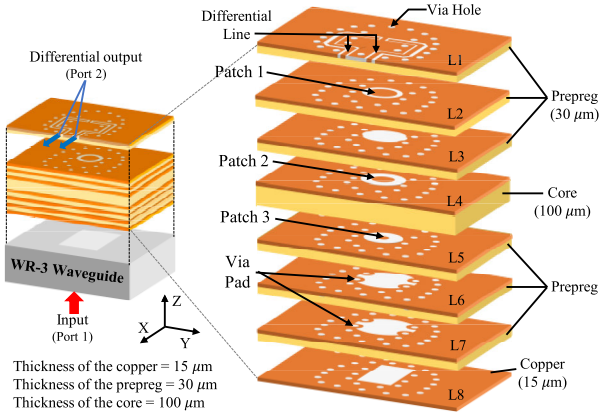

FIGURE 1. Configuration of the waveguide-to-differential-line transition.

The excited field at the patch on L2 was strongly coupled with the signal lines of the differential lines on top L1.

The detailed design of each copper layer is shown in Fig. 2. The metal L8 is in direct contact with the bottom waveguide. Therefore, the aperture is rectangular, and its size is smaller than that of the waveguide cross-section for tolerance in assembly. The apertures on L2–L7 are circular and transformed into the TE_{11} mode, which forms a circular cavity in the multi-layer substrate. The size of the circular aperture gradually decreases from L7–L5. Next, the size of the circular patch increases from L5–L2 for a smooth flow of the electromagnetic wave from the waveguide to the upper layers for broadband characteristics, as shown in Fig. 3. The sizes of the circular apertures on L6 and L7 were designed to balance the mode transformation and prevent higher-order modes. To connect the via holes between L8 surrounding the rectangular aperture and L6 and L7 surrounding the circular apertures via pads are necessary in the inner region of the circular apertures.

The outer conductor of each patch was operated on the ground. The simulated electric field on each layer is shown in Fig. 4. It was confirmed that the electric field of the TE_{10} mode on L8 transformed into the TE_{11} mode in the quasi-circular waveguide on L6 and L7. Patch 3 on L5 was excited, and a strong electric field was generated on both sides of the patch. Patch 2 was excited in the same manner as Patch 3. These two patches are required for a strong coupling between both planes of the thick core layer. The field passes through the aperture on L3. The aperture sizes of L2–L4 were almost the same. However, the size of Patch 3 was smaller, the size of Patch 2 was larger, and Patch 1 was the largest. Therefore, the gap between the patch and the ground gradually decreased from lower to upper to increase the bandwidth. The cavity structure is anticipated to yield multiple resonances. Leveraging these principles, we have extended the bandwidth of reflection below -10 dB to encompass the range of 218.5–314.5 GHz. In our analysis, we observed multimode resonant frequencies at 226 GHz, 278 GHz, and 304 GHz. To validate the impact of multi-transmission modes on the transition characteristics, we conducted a parametric study,

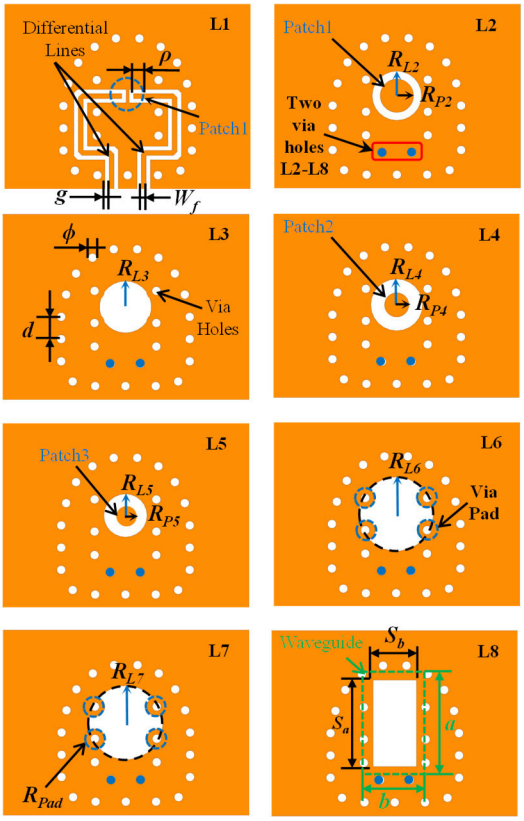

FIGURE 2. Top views of each layer with the parameters for the proposed transition.

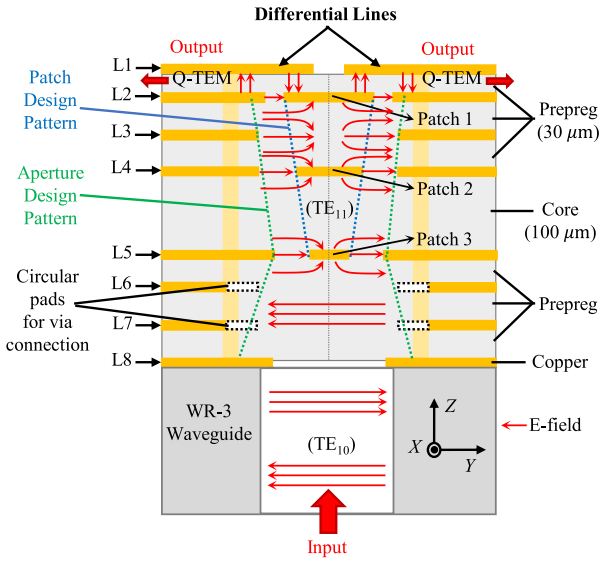

FIGURE 3. Cross-sectional view of proposed transition.

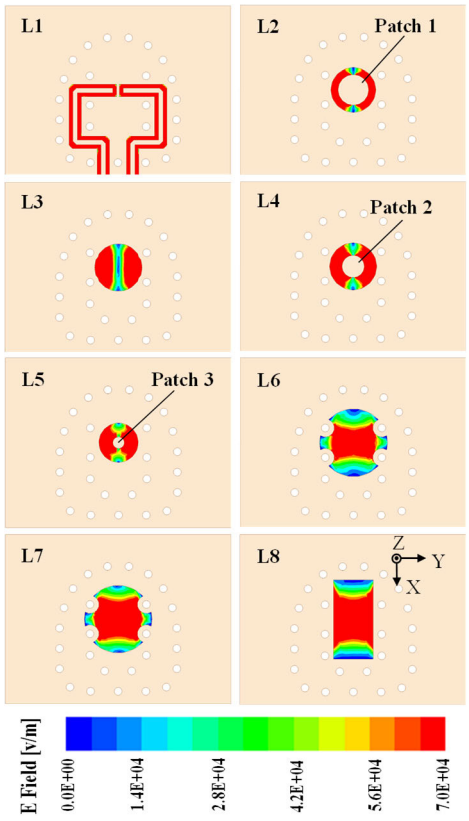

FIGURE 4. Simulated electric field distribution on the metal layer n (n = 1, 2, ..., 8) of the proposed transition at 250 GHz.

systematically varying the radius of the circular patches and apertures. A strong electric field was excited on both sides of Patch 1 on L2 in the opposite phase. The signal lines of the differential line were essentially excited at 180° out of phase due to the symmetrical structure, resulting in differential mode operations.

B. GEOMETRY OF MULTI-LAYER SUBSTRATE WITH VIA HOLES

Both the waveguide region and grounded coplanar lines were surrounded by the via-hole arrangement to prevent leakage of the parallel-plate mode between the ground planes. The minimum diameter of the via holes, minimum spacing between adjacent via holes, minimum clearance from the via hole, and pattern edge of the aperture were limited owing to the fabrication process. The via-holes with a diameter of 70 μm are arranged around the waveguides with a center separation of 180 μm. The manufacturing of the substrate, the via-hole positions may vary by up to $\pm$25 μm, and their diameters may vary by up to $\pm$20 μm. The layout of the via holes was designed to minimize the leakage between the via holes, as shown in Fig. 5 (a). The via holes between the signal lines were located at the middle of the two signal lines. However, the via hole spacing was sufficiently large to allow the leakage of electromagnetic waves from the waveguide corners. To prevent the leakage between the via holes at the middle of the signal lines and at the waveguide corners, two via holes were designed at a location nearly under the signal lines from L2–L8 without connecting to L1, as shown in Fig. 5 (b). The via holes did not interfere with the signal lines on L1.

The features of the proposed transition are included in the eight copper patterns with a conductivity (σ) of 5.8×10^7 S/m. The copper plate has a thickness of 15 μm.

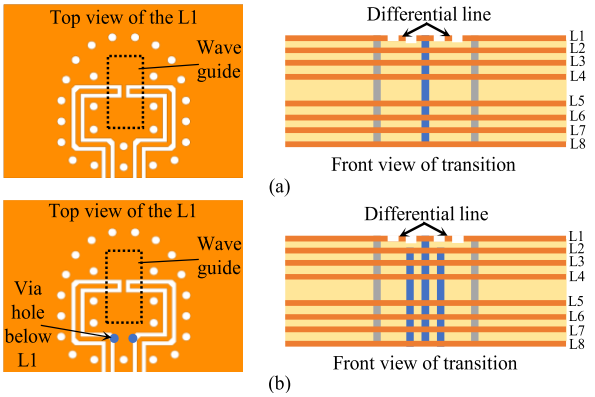

FIGURE 5. Via-hole arrangement (a) with center via hole L1–L8 (b) with two via holes L2–L8.

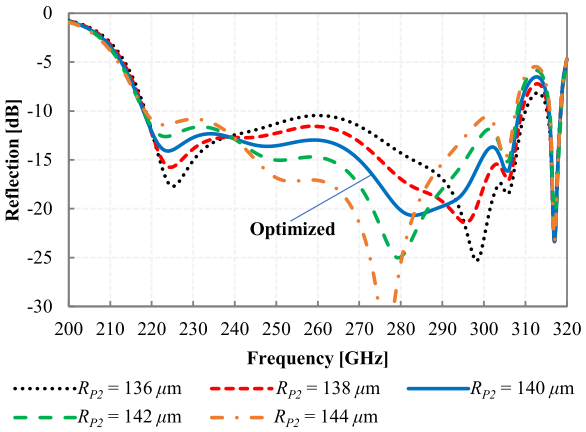

FIGURE 6. Reflection characteristics of the waveguide-to-differential-line transition with center via hole L1–L8 depending on R_{P2}.

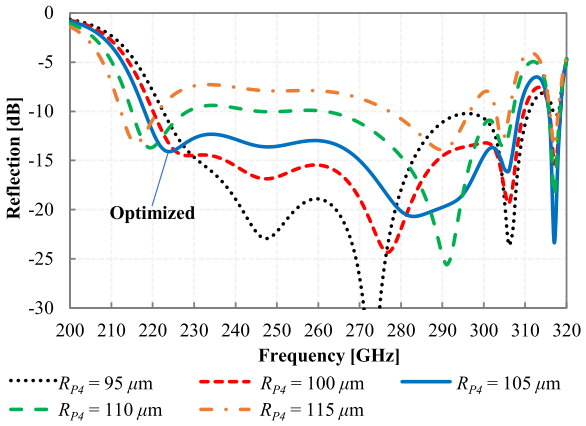

FIGURE 7. Reflection characteristics of the waveguide-to-differential-line transition with center via hole L1–L8 depending on R_{P4}.

The variation in thickness of the copper plate is less than ± 7 μm. A seven- layer dielectric substrate HL972LF-LD [51] (Mitsubishi Gas Chemical Company, Inc.) with a dielectric constant (ε_r) 3.5 and loss tangent (tan δ) 0.003 (based on the datasheet) was used in this paper. Concurrently, three prepreg layers with copper were placed on both sides of the center core layer, forming seven dielectric layers. The thicknesses of the core and the prepreg substrates were 100 μm and 30 μm, respectively. The thickness variation of the core layer is less than ± 15 μm, and the variations of the prepreg layers are less than ± 10 μm. A WR-3 waveguide (864 μm $\times$ 432 μm) was used for the feeding. The dimensions of the design parameters for all the copper layers are shown in Fig. 2. A differential line with width W_f and gap g was inserted into the waveguide region with an overlap ρ on the patch at the top layer, L1. Circular Patch 1 with radius R_{P2} approximately $\lambda g/4$ at 250 GHz (where λg represents the wavelength in the substrate) was located at the center of the circular aperture on Substrate 2. The radius of circular aperture on L2 can be approximately $\lambda g/2$ at 250 GHz. The radius of Circular Patch 2 and Circular Patch 3 are smaller than the radius of Circular Patch 1. Circular Patch 2 with radius R_{P4} and circular Patch 3 with radius R_{P5} were placed at the center of the circular apertures on both sides of the thick-core substrate for strong coupling. Following the arrangement of elements within their layers and assessing their interactions with the ground planes, we conducted parametric optimization to adjust size and gap dimensions. The rectangular aperture $S_a \times S_b$ on L8 was slightly smaller than that on the WR-3 waveguide.

III. PARAMETRIC ANALYSIS AND DISCUSSION

This section presents the numerical investigations of the multi-layer waveguide-to-differential-line transition using the finite element electromagnetic simulator Ansys HFSS [52]. Furthermore, parameters such as the circular patch radius, circular aperture radius of each layer, and via hole arrangement were investigated to study their effects on the frequency response and bandwidth of the transition.

A. TRIPLE CIRCULAR PATCH

This section discusses the effects of the circular patch radius. First, the effect of the radius of circular Patch 1 was studied. The radius of circular Patch 1 (R_{P2}) affects the center resonant frequency observed at approximately 250 GHz. As the radius decreased, the center resonant frequency shifted to a higher as shown in Fig. 6. Next, the effect of radius (R_{P4}) of parasitic Patch 2 was analyzed. When varying R_{P4}, the reflection level changes, as shown in Fig. 7. This implies that the electromagnetic coupling was controlled by changing R_{P4}. As R_{P4} decreases, the radius of circular Patch 2 approaches that of circular Patch 3, enhancing electric field coupling. Thus, significant improvement in impedance matching was observed. Conversely, the reduced radius of circular Patch 2 led to a reduction in the bandwidth. Thus, the optimum value for R_{P4} was 105 μm, providing a broad bandwidth and a suitable matching impedance. This suggests that the matching characteristics can be controlled by changing the radius of circular Patch 2 during the transition.

Finally, the effect of the radius of the parasitic circular Patch 3 (R_{P5}) was analyzed. Circular Patch 3 was crucial for improving the matching impedance at low frequencies.

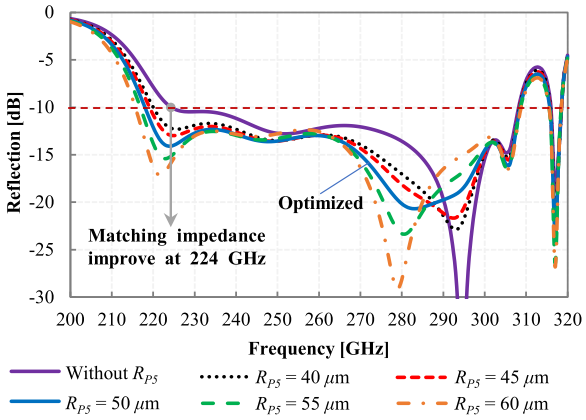

FIGURE 8. Reflection characteristics of the waveguide-to-differential-line transition with center via hole L1–L8 depending on R_{P5}.

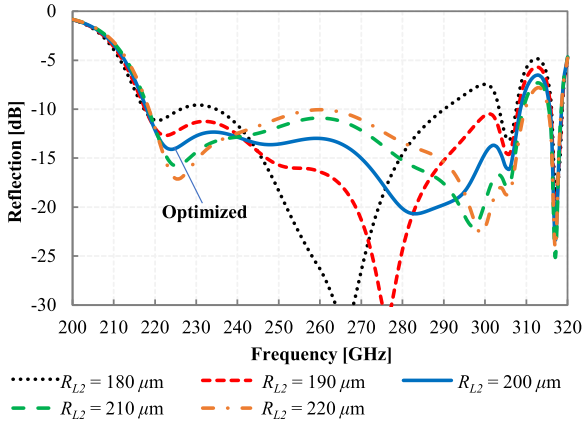

FIGURE 9. Reflection characteristics of the waveguide-to-differential-line transition with center via hole L1–L8 depending on R_{L2}.

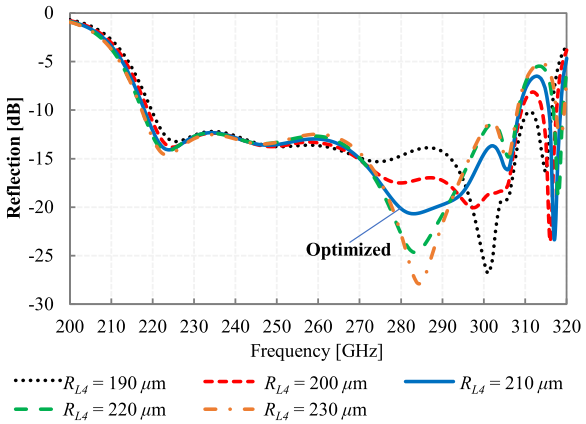

FIGURE 10. Reflection characteristics of the waveguide-to-differential-line transition with center via hole L1–L8 depending on R_{L4}.

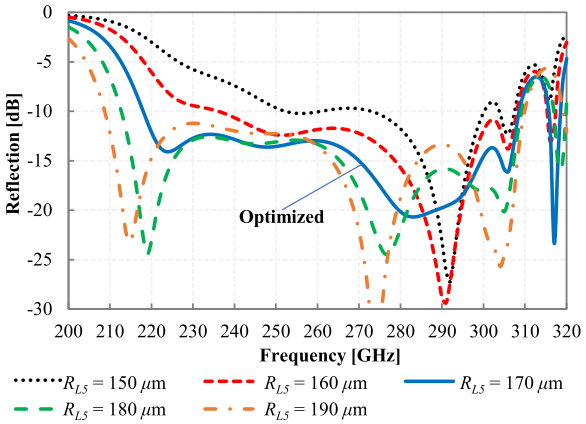

FIGURE 11. Reflection characteristics of the waveguide-to-differential-line transition with center via hole L1–L8 depending on R_{L5}.

The reflection coefficient of the transition depends on R_{P5}, as shown in Fig. 8. The results demonstrated an improved matching impedance at 224 GHz and an increased bandwidth at low frequencies. As R_{P5} increased, the matching impedance at low and high frequencies increased. However, it is worth noting that a slight impact on bandwidth occurs with an increased R_{P5}. The optimal value of R_{P5} was 50 μm.

B. CIRCULAR CAVITY

This section discusses the effects of the aperture on each layer. The effect of the aperture radius on L2 (R_{L2}) was studied to assess its effect on the resonant frequency and bandwidth of the transition. Fig. 9 illustrates the influence of varying R_{L2}, which includes the circular Patch 1, on the reflection coefficient. The aperture size affected the distance between the patches and the aperture edges. When the R_{L2} decreased, the gap with the patch decreased. The bandwidth narrowed with a shifting lower band, owing to the high-Q structure. The effect of the aperture radius on L4 (R_{L4}), which contains circular Patch 2, on the reflection coefficient at high frequencies is shown in Fig. 10. As observed, a decrease in R_{L4} resulted in an improvement in the matching impedance at high frequencies.

Fig. 11 illustrates the dependence of the reflection coefficient on the radius of the aperture on L5 (R_{L5}). The graph demonstrates that increasing R_{L5} significantly improves impedance matching in the low-frequency band. The transmission mode changed drastically at L5 from the waveguide mode to the coaxial mode because of the center patch. Therefore, the dimensions of the apertures R_{L5} and patch R_{P5} are significant parameters for controlling the bandwidth. Fig. 12 shows the reflection coefficient of the transition as the radius of the aperture on L7 (R_{L7}) is varied. The graph demonstrates that the matching impedance at the low-frequency range improves as the radius increases, thereby providing evidence that the aperture radius significantly influences the reflection coefficient level. In conclusion, R_{L2} regulates the reflection coefficient level of the transition across the entire frequency range. R_{L4} governs the reflection coefficient level of the transition at high frequencies, whereas R_{L5} and R_{L7} determine the reflection levels of the transition in the low-frequency range.

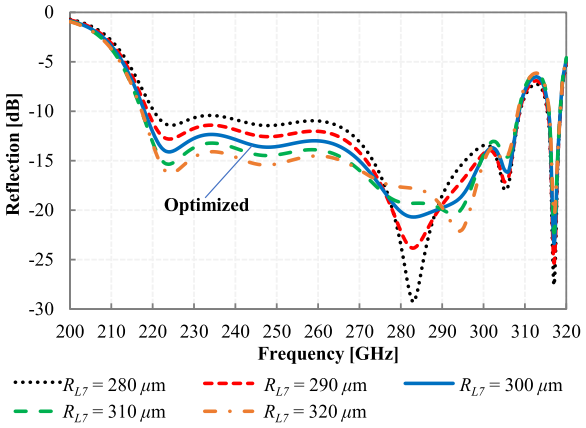

FIGURE 12. Reflection characteristics of the waveguide-to-differential-line transition with center via hole L1–L8 depending on R_{L7}.

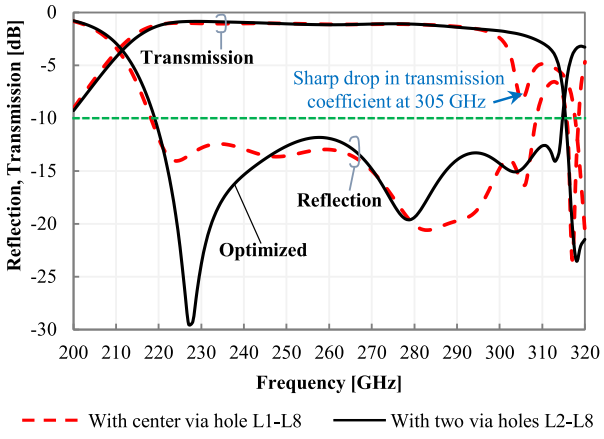

FIGURE 13. Comparison of the scattering characteristics of transition with center via hole L1-L8 and with two via holes L2-L8.

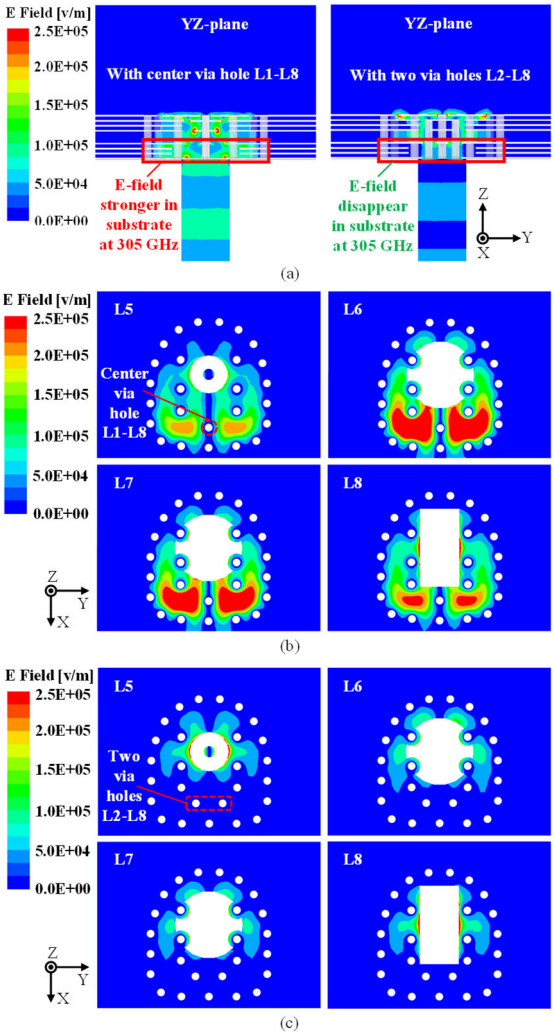

FIGURE 14. Simulated electric field distribution of the proposed transition at 305 GHz (a) Electric field distribution on the YZ-plane of the waveguide center (b) Electric field distribution of the transition from L5–L8 of the multi-layer substrates with center via hole L1–L8 (c) Electric field distribution of the transition from L5–L8 of the multi-layer substrates with two via holes L2–L8.

C. VIA-HOLE ARRANGEMENT

The via-hole spacing against wavelength is wider in the higher-frequency band. This subsection describes the enhancement of the transmission and reflection coefficients at high frequencies by improving the via-hole arrangement. In response to the identified issue, the rearrangement of the via holes is discussed in Section II and shown in Fig. 5. The layout of the via holes was designed to minimize the leakage between the via holes. Fig. 13 shows the transmission and reflection coefficients of these transitions. An analysis was conducted to identify the factors contributing to the decrease in the transmission coefficient at high frequencies over 300 GHz by examining the electric field distribution on each transition layer. Fig. 14 illustrates the electric field distribution of the proposed transition at 305 GHz. Fig. 14 (a) shows the electric field distribution on the *YZ*-plane, including the center axis of the waveguide, indicating a stronger electric field in the substrates from L5–L8. Consequently, resonance occurs at a frequency of 305 GHz, leading to a decrease in the transmission coefficient at this frequency, as depicted by the red dashed line in Fig. 13. It was observed that the inclusion of two via holes in L2–L8 effectively eliminates the strong electric field. To demonstrate the preventive effect of the via hole arrangement on the electric field leakage, Figs. 14 (b) and 14 (c) illustrate the electric field distribution of the transition from L5–L8 in the multi-layer substrates with a center via hole in L1–L8 and two via holes in L2–L8. The results indicate that the via-hole arrangement, specifically with two via holes in L2–L8, effectively prevents leakage and resonance at 305 GHz. The proposed arrangement reduced the via-hole pitch and positioned the via holes to cover the waveguide connections. Consequently, the transmission coefficient was improved, which is evident from the enhancement shown by the black dashed line in Fig. 13.

Table 1 presents all the parameters of the proposed transitions obtained through this optimization process after conducting a comprehensive study on the impact of various transition parameters and subsequent optimizations. Except

TABLE 1. Optimized parameters of the proposed transition.

Name	Description	Value
ε_r	Relative permittivity	3.5
δ	Loss tangent	0.003
W_T	Total width of the transition	1.5 mm
L_T	Total length of the transition	1.5 mm
a	Broad wall length of the waveguide	864 μm
b	Narrow wall length of the waveguide	432 μm
ϕ	Diameter of via hole	70 μm
d	Distance between via hole (Pitch)	180 μm
W_f	Width of differential line	40 μm
g	Width of gap	35 μm
ρ	Overlap length of inserted probe	87.5 μm
R_{P2}	Radius of circular Patch 1	135 μm
R_{P4}	Radius of circular Patch 2	98 μm
R_{P5}	Radius of circular Patch 3	50 μm
R_{L2}	Radius of circular aperture on L2	200 μm
R_{L3}	Radius of circular aperture on L3	210 μm
R_{L4}	Radius of circular aperture on L4	210 μm
R_{L5}	Radius of circular aperture on L5	175 μm
R_{L6}	Radius of circular aperture on L6	300 μm
R_{L7}	Radius of circular aperture on L7	300 μm
R_{Pad}	Radius of circular pad for via	80 μm
S_a	Broad wall length of aperture on L8	700 μm
S_b	Narrow wall length of aperture on L8	350 μm
	Thickness of the copper	15 μm
	Thickness of the prepreg	30 μm
	Thickness of the core	100 μm

for three parameters, namely, the radius of circular Patch 1 (R_{P2}), the radius of circular Patch 2 (R_{P4}), and the radius of the circular aperture on L5 (R_{L5}), all the other parameters remained unchanged between the transitions with a center via hole in L1–L8 and with two via holes in L2–L8. The proposed transition introduces the following parameter values: $R_{P2} = 140\ \mu$m, $R_{P4} = 104\ \mu$m, and $R_{L5} = 170\ \mu$m.

IV. EXPERIMENTAL PERFORMANCES

This section presents the validated simulation results of the proposed transition that were obtained by conducting measurements on the fabricated transitions. We focused on measuring the transmission loss and reflection characteristics.

A. FABRICATION AND MEASUREMENT SETUP

A back-to-back configuration was employed to assess the transmission line losses, characteristics, and efficiencies of the proposed transitions. The fabrication accuracy from the company is shown in Table 2. The setup of the measurement system is shown in Fig. 15. The measured transitions were positioned on a metal jig connected to the waveguide. The

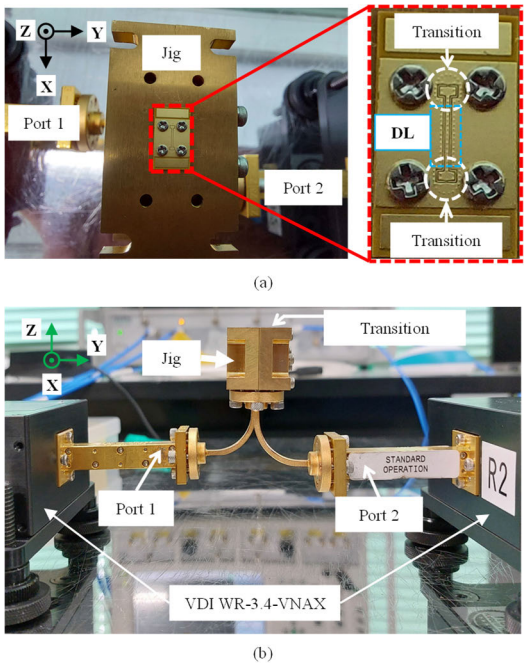

FIGURE 15. Experimental setup of the transition (a) top view (b) side view.

measurement setup involved a differential line connecting two identical transitions with the same geometrical parameters as those of the fabricated substrate. The substrate was mounted on a metal jig, and the waveguides were connected at both terminals and attached to the flange of a standard waveguide (WR-3), as shown in Fig. 15 (a). A choke structure was built around the waveguide on the jig surface to reduce leakage from the gap between the substrate and the jig. The substrate was fixed at a particular position with high precision using a small screw with a diameter of 1 mm. The measurement accuracy was ensured through repetition of the assembly and measurements. Millimeter-wave extension modules VDI WR-3.4-VNAX were connected to a vector network analyzer (ANRITSU MS4647B), as shown in Fig. 15 (b). The two ports of the standard waveguide, which extend from the millimeter-wave module, were calibrated using a WR-3 Anritsu waveguide calibrator model SM6567 at the waveguide-connected plane within the metal jig. The reflection and transmission characteristics encompassing the waveguide within the jig and the transmission line between the two transitions were measured. A vector network analyzer equipped with a time-gate domain function was employed to measure the scattering parameters and mitigate the occurrence of multiple reflections [53]. The entire frequency band of WR-3, ranging from 220 to 320 GHz, was utilized to achieve high time resolution.

To evaluate the insertion loss of each transition accurately, the losses of the differential line between the transitions and waveguides within the jig were measured to determine the required compensation. A study focused on investigating losses in transmission line structures on package substrates

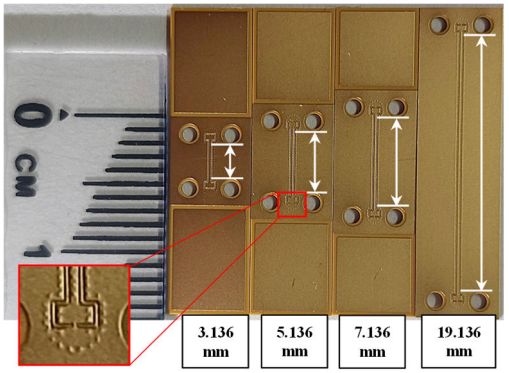

FIGURE 16. Fabricated substrates for different lengths of the transmission line and an enlarged view of the proposed transition (left).

TABLE 2. Design values and fabrication accuracies of the multilayer substrate.

	Design value	Accuracy
Thickness of the core	100 μm	±15 μm
Thickness of the prepreg	30 μm	±10 μm
Thickness of the copper	15 μm	±7 μm
Via diameter	70 μm	±20 μm
Via position	N/A	±25 μm
Pattern width of the signal lines	40 μm	±10 μm
Gap	35 μm	±10 μm
Rounded corner	10 μm	N/A

tailored for the 100 GHz to 300 GHz frequency range. The performance of these transmission lines was evaluated through a combination of analytical and experimental methods, as implemented in [49] and [54]. To obtain the transmission loss of the differential line, transitions with back-to-back configurations connected by differential lines of different lengths were fabricated as shown in Fig. 16. The lengths of the transmission lines were selected as 3.136, 5.136, 7.136, and 19.136 mm to evaluate the transmission loss of the differential line accurately. Fig. 17 illustrates the transmission loss of the differential line, assessed by examining the slopes of curves derived from transmission measurements with differential lines of four different lengths at 230, 250, and 270 GHz. The assessment reveals a transmission loss of approximately 0.8 dB/mm at 250 GHz. Fig. 18 illustrates the individual losses of each component for estimating the insertion loss of a single transition. The measured transmission of the back-to-back of two transitions, including transmission line and jig from Port 1 to Port 2, is represented by the black dashed line. The purple dashed line represents the 3.136 mm transmission line loss, estimated from the difference in measured transmissions for the back-to-back transition of four lengths, as shown in Fig. 16. Additionally, the transmission with waveguide losses in the jig, indicated by the green dashed line, was obtained through jig measurement. The loss of the waveguide in the jig was measured by connecting two identical jigs. The losses of the two waveguides in the jigs

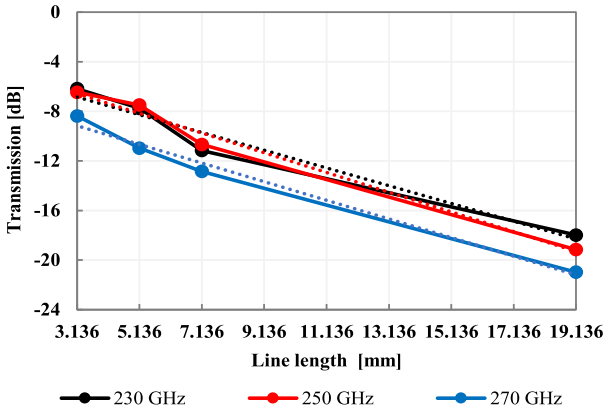

FIGURE 17. Measured transmission of the fabricated transition with four different line lengths.

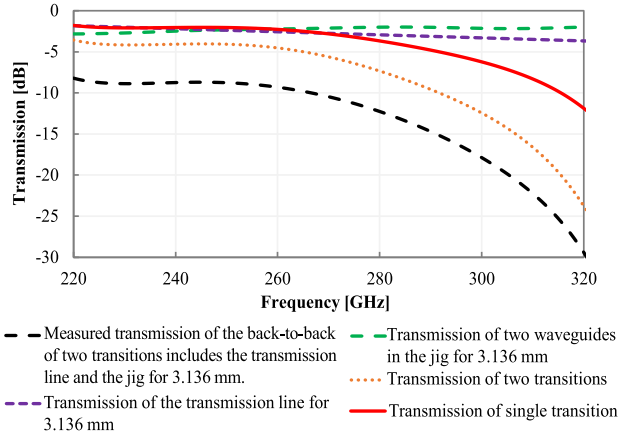

FIGURE 18. Transmission characteristics at each correction process of the proposed transition.

were measured as 1.8 dB at 250 GHz, and the loss of the single waveguide in the jig was estimated to be 0.9 dB by dividing the measured transmission of the two jigs by two. Finally, the transmission coefficient of the single transition was evaluated from the transmission of the entire structure with a differential line of 3.136 mm by de-embedding the jig and differential line losses at every frequency point across the entire frequency band, is represented by the red solid line.

B. MEASUREMENT RESULTS

The measured and simulated scattering parameters for the waveguide-to-differential-line transition are shown in Fig. 19. The measurement process used the WR-3 standard equipment, which covered the entire frequency band ranging from 220 to 320 GHz. The simulation results for the transition with two via holes in L2–L8 indicate a bandwidth of reflection coefficient less than −10 dB, which spans 95.6 GHz (35.8%). The simulated transmission coefficient of the transition with two via holes in L2–L8 at the center frequency of 250 GHz was −1.0 dB. Regarding the measured results, although the lower band edge could not be observed because of the limit of the WR-3 band, the bandwidth of reflection

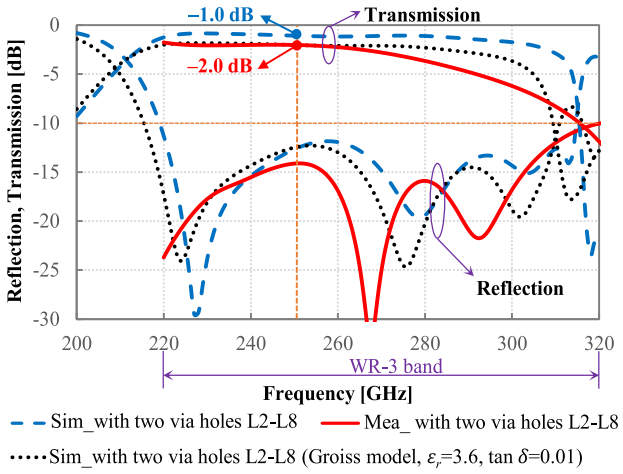

FIGURE 19. Simulated and measured scattering parameter results of the waveguide-to-differential-line transition.

lower than −10 dB from the simulated lower band edge to the measured band edge was 100.0 GHz (37.0%). The measured transmission coefficient at the design frequency of 250 GHz was −2.0 dB.

It is evident from the graph that the measured reflection coefficient shifted to lower frequencies and the reflection level was deferred. This shift can be attributed to the imperfections in the size and position of the via hole as well as uneven substrate thickness. Furthermore, the measured dielectric constant of the fabricated substrate exceeded the reference value provided in the datasheet, with a value of approximately 3.6 at 250 GHz. The measured reflection level at a high resonant frequency is higher than the simulation. The reflection level decreases due to transmission loss. This discrepancy could be attributed to imperfections in the size and placement of the patch, as well as misalignment between layers during the fabrication process.

The measured transmission coefficient results differ from the simulation results mainly because of the surface roughness of the copper sticking to the substrate. The average surface roughness (R_a) utilized in fabrication was approximately 0.3 μm. R_a is the arithmetic average of the absolute values of the profile heights over the evaluation length. This information was sourced from the fabrication company. The skin depth on the copper surface was 0.13 μm based on the theoretical calculations performed at 250 GHz, which is nearly the same dimension as the surface roughness. Therefore, it is suggested that surface roughness significantly influences conductor loss. Additionally, the measured loss tangent of the fabricated substrate exceeded the reference value provided in the datasheet, with a value of approximately 0.01 at 250 GHz. The relative permittivity and loss tangent of the substrate were determined using the Fabry-Perot resonator method within the frequency range of 220 GHz to 320 GHz. Furthermore, multiple factors including fabrication tolerance and mechanical assembly errors can decrease the transmission coefficient. These factors are critical in the

TABLE 3. Comparison of waveguide-to-microstrip transitions.

Ref.	f_c (GHz)	BW_{rel} (%)	S_{11} (dB)	S_{21} (dB)	Interface	Structure
[31]	10.5	47.6	−15	−0.95	CPW	Back-to-Back
[32]	33	40.9	−18.5	−0.26	SSL	Single
[33]	33	44.0	−12	−0.34	SISL	Single
[39]	33	40.6	−15	−0.4	Differential	Single
[40]	80	20.2	−10	−1.92	Differential	Single
[41]	122	11.8	−10	−1.63*	Differential	Back-to-Back
[42]	120	25.0	−10	−1.8	Differential	Single
[43]	60	20.0	−10	−0.8	Differential	Single
[49]	275	23.6	−10	−2.6	Differential	Single
This work	250	37.0	−10	−2.0	Differential	Single

*Simulation result

THz frequency bands, particularly when dealing with multilayered structures. For surface roughness analysis, HFSS offers a modified version of the Morgan-Hammerstad empirical fit, referred to as the Groiss equation. The Groiss model [55] assumes that the high-frequency current adheres to the surface profile. This adherence is measured by deviations in the direction of the normal vector from its ideal form. Large deviations indicate a rough surface, while small ones suggest a smooth surface. The simulation results integrate a Groiss model with an average surface roughness (R_a) of 0.3 μm, as the actual value from the fabrication is not available. Coupled with the measured dielectric constant of 3.6 and a loss tangent of 0.01, they are depicted by the black dotted line in Fig. 19. It can be observed that surface roughness and loss tangent affect the transmission, particularly at high frequencies. It aligns with [54] that as the frequency increases, the loss tangent and the dielectric constant of the substrate also increase, resulting in an increase in loss at high frequencies. Moreover, an increase in the dielectric constant causes the reflection coefficient to shift to low frequencies.

C. COMPARISON OF PERFORMANCES

Table 3 presents the performance comparison between the proposed waveguide-to-microstrip transition and previously published results. However, the design frequencies and techniques used in this paper differ from those of the proposed method. For instance, a transition from CPW to air- filled rectangular waveguide was proposed in [31]. A suspended stripline to air-filled rectangular waveguide transition was presented in [32], and a substrate integrated suspended line (SISL) to rectangular waveguide transition was developed [33]. While these transitions exhibit a wide bandwidth, their operation is low frequencies. Therefore, comparisons with the most similar methods are provided to evaluate the effectiveness of this paper, focusing mainly on the waveguide-to-differential-line transitions [39], [40], [41], [42], [43], but the bandwidth is still not wide. For [49], the bandwidth of the reflections less than −10 dB was 66.3 GHz (23.6%) and the measured transmission coefficient for the

single transition was −2.6 dB at 275 GHz. For this work, the frequency bandwidth of 100 GHz (37.0%) at the reference S_{11} below −10 dB was consistent with the waveguide standard of WR-3. The transmission coefficient of the single transition from the measured was −2.0 dB at 250 GHz and more than −3 dB at frequencies higher than 280 GHz. These results are comparable to those of other designs.

V. CONCLUSION

A multi-layer waveguide-to-differential-line transition with a circular cavity and triple circular patch was proposed. The multi-layer waveguide-to-differential-line transition operates under a combination of triple-stacked patch arrangements and circular cavity structures. The transition had a wide bandwidth of 100.0 GHz (37.0%). The multi-layer waveguide-to-differential-line transition measured with circular cavity and triple patch showed a transmission coefficient of −2.0 dB at the center frequency of 250 GHz. The measured performance confirmed the feasibility of the multi-layer waveguide-to-differential-line transition. It is suitable for applications in practical terahertz systems.

ACKNOWLEDGMENT

The measured dielectric constant of the substrate was provided from KYOCERA Corporation and NICT.

REFERENCES

[1] H.-J. Song and T. Nagatsuma, "Present and future of terahertz communications," *IEEE Trans. Terahertz Sci. Technol.*, vol. 1, no. 1, pp. 256–263, Sep. 2011, doi: 10.1109/TTHZ.2011.2159552.

[2] H.-J. Song, K. Ajito, A. Wakatsuki, Y. Muramoto, N. Kukutsu, Y. Kado, and T. Nagatsuma, "Terahertz wireless communication link at 300 GHz," in *Proc. IEEE Int. Topical Meeting Microwave Photon.*, Oct. 2010, pp. 42–45, doi: 10.1109/MWP.2010.5664230.

[3] T. Nagatsuma, H.-J. Song, Y. Fujimoto, K. Miyake, A. Hirata, K. Ajito, A. Wakatsuki, T. Furuta, N. Kukutsu, and Y. Kado, "Giga-bit wireless link using 300–400 GHz bands," in *Proc. Int. Topical Meeting Microwave Photon.*, Valencia, Spain, Oct. 2009, pp. 1–4.

[4] H.-J. Song, J.-Y. Kim, K. Ajito, M. Yaita, and N. Kukutsu, "Fully integrated ASK receiver MMIC for terahertz communications at 300 GHz," *IEEE Trans. Terahertz Sci. Technol.*, vol. 3, no. 4, pp. 445–452, Jul. 2013, doi: 10.1109/TTHZ.2013.2252954.

[5] G. Ducournau, P. Szriftgiser, F. Pavanello, E. Peytavit, M. Zaknoune, D. Bacquet, A. Beck, T. Akalin, J.-F. Lampin, and J.-F. Lampin, "THz communications using photonics and electronic devices: The race to data-rate," *J. Infr. Millim., Terahertz Waves*, vol. 36, no. 2, pp. 198–220, Feb. 2015, doi: 10.1007/s10762-014-0112-x.

[6] H.-J. Song, T. Tajima, T. Kosugi, H. Hamada, A. E. Moutaouakil, H. Sugiyama, H. Matsuzaki, M. Yaita, S. Kodama, and O. Kagami, "Demonstration of KIOSK data downloading system at 300 GHz based on InP MMICs," in *Proc. IEEE Int. Symp. Radio-Freq. Integr. Technol. (RFIT)*, Aug. 2015, pp. 52–54, doi: 10.1109/RFIT.2015.7377884.

[7] W. Jiang, B. Han, M. A. Habibi, and H. D. Schotten, "The road towards 6G: A comprehensive survey," *IEEE Open J. Commun. Soc.*, vol. 2, pp. 334–366, 2021, doi: 10.1109/OJCOMS.2021.3057679.

[8] S. Suyama, T. Okuyama, Y. Kishiyama, S. Nagata, and T. Asai, "A study on extreme wideband 6G radio access technologies for achieving 100Gbps data rate in higher frequency bands," *IEICE Trans. Commun.*, vols. E104–B, no. 9, pp. 992–999, Sep. 2021, doi: 10.1587/transcom.2020fgi0002.

[9] E. Marchetti, L. Daniel, E. G. Hoare, F. Norouzian, M. Cherniakov, and M. Gashinova, "Radar reflectivity of a passenger car at 300 GHz," in *Proc. 19th Int. Radar Symp. (IRS)*, Jun. 2018, pp. 1–7, doi: 10.23919/IRS.2018.8448009.

[10] S. Hara, R. Dong, S. Lee, K. Takano, N. Toshida, A. Kasamatsu, K. Sakakibara, T. Yoshida, S. Amakawa, and M. Fujishima, "A 76-Gbit/s 265-GHz CMOS receiver with WR-3.4 waveguide interface," *IEEE J. Solid-State Circuits*, vol. 57, no. 10, pp. 2988–2998, Oct. 2022, doi: 10.1109/JSSC.2022.3179560.

[11] S. Hara, R. Dong, S. Lee, K. Takano, N. Toshida, S. Tanoi, T. Hagino, M. H. Mubarak, N. Sekine, I. Watanabe, A. Kasamatsu, K. Sakakibara, S. Kubo, S. Miura, Y. Umeda, T. Yoshida, S. Amakawa, and M. Fujishima, "A 76-Gbit/s 265-GHz CMOS receiver," in *Proc. IEEE Asian Solid-State Circuits Conf. (A-SSCC)*, Nov. 2021, pp. 1–3, doi: 10.1109/A-SSCC53895.2021.9634780.

[12] T. Tajima, H.-J. Song, M. Yaita, K. Ajito, and N. Kukutsu, "300-GHz LTCC horn antennas based on antenna-in-package technology," in *Proc. Eur. Microwave Conf.*, Oct. 2013, pp. 231–234.

[13] Y. Deguchi, K. Sakakibara, N. Kikuma, and H. Hirayama, "Millimeter-wave microstrip-to-waveguide transition operating over broad frequency bandwidth," in *IEEE MTT-S Int. Microwave Symp. Dig.*, Jun. 2005, pp. 2107–2110, doi: 10.1109/MWSYM.2005.1517163.

[14] K. Sakakibara, M. Hirono, N. Kikuma, and H. Hirayama, "Broadband and planar microstrip-to-waveguide transitions in millimeter-wave band," in *Proc. Int. Conf. Microwave Millim. Wave Technol.*, vol. 3, Apr. 2008, pp. 1278–1281, doi: 10.1109/ICMMT.2008.4540667.

[15] J. Svedin, T. Pellikka, and L.-G. Huss, "A direct transition from microstrip to waveguide for millimeter-wave MMICs using LTCC," in *Proc. Asia–Pacific Microwave Conf.*, Dec. 2011, pp. 102–105.

[16] N. Dib and A. Omar, "Analysis of grounded coplanar waveguide fed patches and waveguides," in *Proc. IEEE Antennas Propag. Soc. Int. Symp. Dig.*, Jul. 1109, pp. 2530–2533, doi: 10.1109/APS.1997.625517.

[17] N. Dib and A. Omar, "FDTD analysis of a new transition from coplanar waveguide to rectangular waveguide," *Microwave Opt. Technol. Lett.*, vol. 29, no. 3, pp. 199–201, May 2001.

[18] H. Iizuka, T. Watanabe, K. Sato, and K. Nishikawa, "Millimeter-wave microstrip line to waveguide transition fabricated on a single layer dielectric substrate," *IEICE Trans. Commu.*, vol. 85, no. 6, pp. 1169–1177, 2002.

[19] Y. Ishikawa, K. Sakakibara, Y. Suzuki, and N. Kikuma, "Millimeter-wave topside waveguide-to-microstrip transition in multilayer substrate," *IEEE Microwave Wireless Compon. Lett.*, vol. 28, no. 5, pp. 380–382, May 2018, doi: 10.1109/LMWC.2018.2812125.

[20] Y. Xiao, H. Luo, and H. Sun, "A novel millimeter-wave transition fromwaveguide to microstrip line," in *Proc. IEEE Int. Conf. Microwave Technol. Comput. Electromagn.*, Qingdao, China, Aug. 2013, pp. 111–114, doi: 10.1109/ICMTCE.2013.6812401.

[21] A. Abdellatif, M. Ghassemi, M.-R. Nezhad-Ahmadi, S. Safavi-Naeini, and N. Ghassemi, "Low cost low loss waveguide-fed patch antenna array for automotive radar system," in *Proc. Global Symp. Millimeter-Waves (GSMM)*, Montreal, QC, Canada, May 2015, pp. 1–3, doi: 10.1109/GSMM.2015.7175438.

[22] H. Iizuka, K. Sakakibara, and N. Kikuma, "Millimeter-wave transition from waveguide to two microstrip lines using rectangular patch element," *IEEE Trans. Microwave Theory Techn.*, vol. 55, no. 5, pp. 899–905, May 2007, doi: 10.1109/TMTT.2007.895139.

[23] M. Elsässer, E. M. Navarro, V. Ziegler, and L. Vietzorreck, "Development of a simple broadband microstrip to waveguide transition," in *Proc. Int. Conf. Electromagn. Adv. Appl. (ICEAA)*, Verona, Italy, Sep. 2017, pp. 1700–1703, doi: 10.1109/ICEAA.2017.8065620.

[24] M. Jenning, M. Kurras, and D. Plettemeier, "Waveguide to microstrip transition at 235 GHz," in *Proc. Int. Workshop Antenna Technol. (iWAT)*, Mar. 2010, pp. 1–4, doi: 10.1109/IWAT.2010.5464735.

[25] K. Seo, K. Sakakibara, and N. Kikuma, "Narrow-wall-connected microstrip-to-waveguide transition using V-shaped patch element in millimeter-wave band," *IEICE Trans. Commun.*, vols. E93–B, no. 10, pp. 2523–2530, Oct. 2010, doi: 10.1587/transcom.e93.b.2523.

[26] K. Murase, K. Sakakibara, N. Kikuma, and H. Hirayama, "Design of via-less planer microstrip-to-waveguide transition with choke structure," in *Proc. Int. Symp. Antennas Propag. (ISAP)*, Oct. 2012, pp. 267–270.

[27] B. Yuan, P. Wu, Z. Yu, and C. Hao, "Wideband end-wall transition from microstrip to waveguide with via-less choke structure for terahertz application," *IEEE Trans. Terahertz Sci. Technol.*, vol. 12, no. 3, pp. 317–320, May 2022, doi: 10.1109/TTHZ.2022.3163356.

[28] N. Thanh Tuan, K. Sakakibara, and N. Kikuma, "Bandwidth extension of planar microstrip-to-waveguide transition by controlling transmission modes through via-hole positioning in millimeter-wave band," *IEEE Access*, vol. 7, pp. 161385–161393, 2019, doi: 10.1109/ACCESS.2019.2952073.

[29] T. Tajima, H.-J. Song, and M. Yaita, "300-GHz microstrip-to-waveguide transition integrated in LTCC," in *IEEE MTT-S Int. Microwave Symp. Dig.*, Jun. 2014, pp. 1–4, doi: 10.1109/MWSYM.2014.6848246.

[30] T. Tajima, H.-J. Song, and M. Yaita, "Design and analysis of LTCC-integrated planar microstrip-to-waveguide transition at 300 GHz," *IEEE Trans. Microwave Theory Techn.*, vol. 64, no. 1, pp. 106–114, Jan. 2016, doi: 10.1109/TMTT.2015.2504474.

[31] Y. Zhao, J. Dong, F. Yin, X. Fang, and K. Xiao, "Broadband coplanar waveguide to air-filled rectangular waveguide transition," *Electronics*, vol. 11, no. 7, p. 1057, Mar. 2022, doi: 10.3390/electronics11071057.

[32] J. Dong, H. Peng, Y. Liu, H. Lin, and T. Yang, "Broadband suspended stripline to air-filled rectangular waveguide transition," *Electron. Lett.*, vol. 51, no. 23, pp. 1886–1888, Nov. 2015, doi: 10.1049/el.2015.2743.

[33] Y. Chen, K. Ma, and Y. Wang, "A Ka-band substrate integrated suspended line to rectangular waveguide transition," *IEEE Microwave Wireless Compon. Lett.*, vol. 28, no. 9, pp. 744–746, Sep. 2018, doi: 10.1109/LMWC.2018.2849203.

[34] H. Y. Lee, D. S. Jun, S. E. Moon, E. K. Kim, J. H. Park, and K. H. Park, "Wideband aperture coupled stacked patch type microstrip to waveguide transition for V-band," in *Proc. Asia–Pacific Microwave Conf.*, Dec. 2006, pp. 360–362, doi: 10.1109/APMC.2006.4429440.

[35] A. Meyer, S. Karau, and M. Schneider, "Broadband stacked-patch transition from microstrip line to circular dielectric waveguide for dual-polarized applications at W-band frequencies," in *Proc. 49th Eur. Microwave Conf. (EuMC)*, Paris, France, Oct. 2019, pp. 440–443, doi: 10.23919/EuMC.2019.8910938.

[36] M. Ortner, Z. Tong, and T. Ostermann, "A millimeter-wave wide-band transition from a differential microstrip to a rectangular waveguide for 60 GHz applications," in *Proc. 5th Eur. Conf. Antennas Propag. (EUCAP)*, Apr. 2011, pp. 1946–1949.

[37] H. A. Diawuo and Y.-B. Jung, "Waveguide-to-stripline transition design in millimeter-wave band for 5G mobile communication," *IEEE Trans. Antennas Propag.*, vol. 66, no. 10, pp. 5586–5589, Oct. 2018, doi: 10.1109/TAP.2018.2854364.

[38] S. Mariyama, K. Sakakibara, N. Kikuma, and Y. Sugimoto, "Design of broadband transition from hollow waveguide to differential line on multi-layer dielectric substrates," in *Proc. Int. Conf. Emerg. Technol. Commu. (ICETC)*, Dec. 2020, p. 1.

[39] Z. Yang, T. Yang, Y. Liu, and H. Peng, "A compact and broadband differential microstrip line to rectangular waveguide transition using dipole antenna," *J. Infr. Millim. Terahertz Waves*, vol. 37, no. 6, pp. 582–591, Jun. 2016, doi: 10.1007/s10762-016-0253-1.

[40] T. Yuasa, T. Oba, Y. Tahara, Y. Morimoto, T. Owada, and M. Miyazaki, "A millimeter wave wideband differential line to waveguide transition using short ended slot line," in *Proc. 44th Eur. Microwave Conf.*, Oct. 2014, pp. 1004–1007, doi: 10.1109/EUMC.2014.6986607.

[41] R. Hasan, W. A. Ahmed, J.-H. Lu, H. J. Ng, and D. Kissinger, "*F*-band differential microstrip patch antenna array and waveguide to differential microstrip line transition for FMCW radar sensor," *IEEE Sensors J.*, vol. 19, no. 15, pp. 6486–6496, Aug. 2019, doi: 10.1109/JSEN.2019.2909935.

[42] P. Hügler, T. Chaloun, and C. Waldschmidt, "A wideband differential microstrip-to-waveguide transition for multilayer PCBs at 120 GHz," *IEEE Microwave Wireless Compon. Lett.*, vol. 30, no. 2, pp. 170–172, Feb. 2020, doi: 10.1109/LMWC.2019.2958208.

[43] S. Churkin, A. Mozharovskiy, A. Myskov, A. Artemenko, and R. Maslennikov, "Top-layer wideband transition from waveguide to planar differential line for 60 GHz applications," in *Proc. 48th Eur. Microwave Conf. (EuMC)*, Sep. 2018, pp. 663–666, doi: 10.23919/EUMC.2018.8541701.

[44] K. Lomakin, L. Engel, J. Fleischmann, and G. Gold, "Additively manufactured wavemode transition for broadband E-band applications," in *IEEE MTT-S Int. Microwave Symp. Dig.*, Jun. 2021, pp. 138–141, doi: 10.1109/IMS19712.2021.9574889.

[45] B. Deutschmann and A. F. Jacob, "A full W-band waveguide-to-differential microstrip transition," in *IEEE MTT-S Int. Microwave Symp. Dig.*, Jun. 2019, pp. 335–338, doi: 10.1109/MWSYM.2019.8700982.

[46] Z. Tong, A. Stelzer, W. Menzel, C. Wagner, R. Feger, and E. Kolmhofer, "A wide band transition from waveguide to differential microstrip lines," in *Proc. Asia–Pacific Microwave Conf.*, Dec. 2008, pp. 1–4, doi: 10.1109/APMC.2008.4957941.

[47] M. Giese, T. Meinhardt, and A. F. Jacob, "Compact wideband single-ended and differential microstrip-to-waveguide transitions at W-band," in *IEEE MTT-S Int. Microwave Symp. Dig.*, Phoenix, AZ, USA, May 2015, pp. 1–4, doi: 10.1109/MWSYM.2015.7167143.

[48] C. López, V. Desmaris, D. Meledin, A. Pavolotsky, and V. Belitsky, "Waveguide-to-Substrate transition based on unilateral substrateless fin-line structure: Design, fabrication, and characterization," *IEEE Trans. Terahertz Sci. Technol.*, vol. 10, no. 6, pp. 668–676, Nov. 2020, doi: 10.1109/TTHZ.2020.3020683.

[49] M. Yamazaki, Y. Sugimoto, K. Sakakibara, and N. Kikuma, "Broadband differential-line-to-waveguide transition in multi-layer dielectric substrates with an X-shaped patch element in 280 GHz band," *IEEE Trans. Microwave Theory Techn.*, vol. 71, no. 6, pp. 1–9, Jan. 2023, doi: 10.1109/TMTT.2022.3232501.

[50] K. Feng, T. Spencer, and J. Watkowski, "Integrated metallization system for high density interconnects and modified semi additive processing," in *Proc. 8th Int. Microsyst., Packag., Assem. Circuits Technol. Conf. (IMPACT)*, Taipei, Taiwan, Oct. 2013, pp. 241–244, doi: 10.1109/IMPACT.2013.6706700.

[51] Mitsubishi Gas Chemical. (Apr. 4, 2024). *Non-Haloganated Low CTE BT Resin Laminate for IC Plastic Packages*. [Online]. Available: https://www.mgc.co.jp/eng/products/sc/btprint/lineup/hfbt.html

[52] *HFSS Help 2023 R1*, Ansoft Corp., Canonsburg, PA, USA, 2023.

[53] Anritsu Company. *Calibration and Measurement Guide VectorStarTM MS464×B Series Microwave Vector Network Analyzer*, ch. 14. Accessed: Apr. 4, 2024. [Online]. Available: https://dl.cdn-anritsu.com/en-us/test-measurement/files/Manuals/Operation-Manual/10410-00317W.pdf

[54] Y. Morishita, K. Takahashi, R. Hasaba, T. Murata, K. Takinami, H. Kitamura, U. Sangawa, T. Tomura, and I. Watanabe, "Comparison between microstrip-line and substrate integrated waveguide on package substrate in 170 GHz and 300 GHz bands," in *Proc. Asia–Pacific Microwave Conf. (APMC)*, Nov. 2022, pp. 196–198, doi: 10.23919/APMC55665.2022.9999775.

[55] S. Groiss, I. Bardi, O. Biro, K. Preis, and K. R. Richter, "Parameters of lossy cavity resonators calculated by the finite element method," *IEEE Trans. Magn.*, vol. 32, no. 3, pp. 894–897, May 1996, doi: 10.1109/20.497385.

CHATCHAI CHOKCHAI (Graduate Student Member, IEEE) was born in Bangkok, Thailand, in 1987. He received the B.S. degree in electronic technology engineering and the M.S. degree in electrical engineering from the King Mongkut's University of Technology, North Bangkok, Thailand, in 2010 and 2013, respectively. He is currently pursuing the Ph.D. degree in electrical and mechanical engineering. His current research interests include the microstrip-to-waveguide transition for millimeter-wave and THz applications.

YOSHIKI SUGIMOTO (Member, IEEE) was born in Fukui, Japan. He received the B.Sc. and M.Sc. degrees from the University of Fukui, Fukui, Japan, in 2013 and 2015, respectively, and the Ph.D. degree from Yokohama National University, Yokohama, Japan, in 2018. From 2018 to 2020, he was with Omron Corporation, where he was involved in the development of wireless power transfer systems and millimeter radar signal processing. In 2020, he joined Nagoya Institute of Technology as an Assistant Professor. His research interests include antenna measurement and scattering problems.

KUNIO SAKAKIBARA (Senior Member, IEEE) was born in Aichi, Japan, in 1968. He received the B.S. degree in electrical and computer engineering from Nagoya Institute of Technology, Nagoya, Japan, in 1991, and the M.S. and D.E. degrees in electrical and electronic engineering from Tokyo Institute of Technology, Tokyo, Japan, in 1993 and 1996, respectively. From 1996 to 2002, he was with Toyota Central Research and Development Laboratories Inc., Nagakute, where he was involved in the development of antennas for automotive millimeter-wave radar systems. From 2000 to 2001, he was a Guest Researcher with the Department of Microwave Techniques, University of Ulm, Ulm, Germany. In 2002, he joined Nagoya Institute of Technology as a Lecturer. Since 2004, he has been an Associate Professor and became a Professor with Nagoya Institute of Technology, in 2012. His current research interests include millimeter-wave antennas and feeding circuits.

HENRY ABU DIAWUO was born in Kumasi, Ghana, in 1991. He received the B.S. degree in telecommunication engineering from the Kwame Nkrumah University of Science and Technology, Kumasi, in 2013, and the M.S. and Ph.D. degrees in electronic engineering from Hanbat National University, Daejeon, South Korea, in 2016 and 2019, respectively. He is currently a Research Associate with the Millimeter-Wave and Terahertz-Wave Wireless System Laboratory, Nagoya Institute of Technology, Nagoya, Japan. His work is focused on active phased array antenna systems for THz Applications. His research interests include active phased array antenna systems and active/passive components in the field of RF and microwave.

NOBUYOSHI KIKUMA (Senior Member, IEEE) was born in Ishikawa, Japan, in 1960. He received the B.S. degree in electronic engineering from Nagoya Institute of Technology, Japan, in 1982, and the M.S. and Ph.D. degrees in electrical engineering from Kyoto University, Japan, in 1984 and 1987, respectively. From 1987 to 1988, he was a Research Associate with Kyoto University. In 1988, he joined Nagoya Institute of Technology, where he has been a Professor, since 2001. His current research interests include adaptive and signal-processing arrays, multipath propagation analysis, mobile and indoor wireless communication, and electromagnetic field theory. He was a recipient of the Fourth Telecommunications Advancement Foundation Award, in 1989.